

This discussion paper is/has been under review for the journal Biogeosciences (BG).
Please refer to the corresponding final paper in BG if available.

Insights into oxygen transport and net community production in sea ice from oxygen, nitrogen and argon concentrations

J. Zhou^{1,2}, B. Delille², F. Brabant¹, and J.-L. Tison¹

¹Laboratoire de glaciologie, DSTE, Université Libre de Bruxelles, Brussels, Belgium

²Unité d'Océanographie chimique, MARE, Université de Liège, Liège, Belgium

Received: 20 December 2013 – Accepted: 24 January 2014 – Published: 4 February 2014

Correspondence to: J. Zhou (jiayzhou@ulb.ac.be)

Published by Copernicus Publications on behalf of the European Geosciences Union.

Title Page

Abstract

Introduction

Conclusions

References

Tables

Figures

⏪

⏩

◀

▶

Back

Close

Full Screen / Esc

Printer-friendly Version

Interactive Discussion

Abstract

We present the evolution of O₂ standing stocks, saturation levels and concentrations in landfast sea ice, collected in Barrow (Alaska), from February to June 2009. The comparison of the standing stocks and saturation levels of O₂ against those of N₂ and Ar suggests that the dynamic of O₂ in sea ice strongly depends on physical processes (gas incorporation and subsequent transport). We then discuss on the use of O₂/Ar and O₂/N₂ to correct for the physical contribution and to determine the biological contribution (NCP) to O₂ supersaturations. We conclude that O₂/Ar suits better than O₂/N₂, because O₂/N₂ is more sensitive due to the relative abundance of O₂, N₂ and Ar, and less biased when gas bubble formation and gas diffusion are maximized. We further estimate the NCP in the impermeable layers during ice growth and in the permeable layers during ice decay. Our results indicate that NCP contributed to a release of carbon to the atmosphere in the upper ice layers, but to an uptake of carbon at sea ice bottom. Overall, seawater (rather than the atmosphere) may be the main supplier of carbon for sea ice microorganisms.

1 Introduction

Sea ice is a porous material with a matrix of pure ice and brine inclusions (Weeks, 2010). The brine inclusions concentrate most of the impurities of the ice, and host micro-organisms that are able to survive to high salinities and low temperatures (Thomas and Dieckmann, 2002). Quantifying the net community production (NCP) – the balance between photosynthesis and respiration – of the microorganisms in sea ice is crucial, because the NCP affects the growth of higher trophic-level species (Arrigo et al., 2010; Brierley and Thomas, 2002; Michel et al., 1996) and the microbial net production of climate-active gases like CO₂ and DMS (Vancoppenolle et al., 2013)

Diverse experimental techniques exist for determining the NCP (see Arrigo et al. (2010) for further details); these are generally derived from seawater studies

BGD

11, 2045–2081, 2014

Insights into oxygen transport and net community production

J. Zhou et al.

Title Page

Abstract

Introduction

Conclusions

References

Tables

Figures

⏪

⏩

◀

▶

Back

Close

Full Screen / Esc

Printer-friendly Version

Interactive Discussion

despite the heterogeneous structure of sea ice in comparison to seawater. A standard technique is to measure the accumulation of algal biomass and its temporal evolution via the measurements of chlorophyll *a* (chl *a*) or particulate organic carbon (POC). Another standard technique is to measure the maximum photosynthetic rate and the photosynthetic efficiency in laboratory. Then, assuming that these photosynthetic parameters still hold for field measurements, we can deduce the changes of biomass based on the concentration of chl *a* and the light intensity from the field. Both standard techniques have one major limitation: they require sea ice extraction and melting, which inevitably modify the growth environment of the microorganisms. Therefore, recent technical developments have privileged in-situ measurements of NCP that minimize the disturbance on sea ice.

The newly-developed techniques for NCP measurements include pulse amplitude modulated (PAM) fluorometry (Glud et al., 2002), O₂ microelectrodes (McMinn and Ashworth, 1998), O₂ micro-optodes (Mock et al., 2002) and O₂ eddy correlation systems (Long et al., 2012). Although these techniques allow in situ measurements, the results may not directly represent the NCP, due to the heterogeneous structure of the ice and to sea ice physical properties (i.e., permeability and brine dynamics). For instance, the PAM fluorescence depends on the spatial distribution of the algal biomass and the optical properties of the ice (Glud et al., 2002). Another example is that the amount of O₂ measured using microsensors depend on whether the sensors were set in brine, ice, gas bubbles or bacterial films (Mock et al., 2002) and whether the ice permeability allows the diffusion of O₂ to the microsensors (Glud et al., 2002). Although the O₂ eddy correlation system seems promising, because of its large footprint in comparison to the other techniques, it may be sensitive to the additional input of O₂ from sea ice due to brine rejection and ice melt (Long et al., 2012). In that context, understanding the dynamic of O₂ within the ice will better constrain the O₂ fluxes at the ice–water interface, obtained with eddy correlation.

In the present study, we describe the dynamic of O₂ in sea ice, based on a time-series of O₂ concentrations within sea ice from ice growth to ice decay. The O₂ mea-

BGD

11, 2045–2081, 2014

Insights into oxygen transport and net community production

J. Zhou et al.

Title Page

Abstract

Introduction

Conclusions

References

Tables

Figures

⏪

⏩

◀

▶

Back

Close

Full Screen / Esc

Printer-friendly Version

Interactive Discussion

in Zhou et al. (2013). In brief, all of the ice cores had similar crystallographic structure, with a dominance of columnar ice that suggests low spatial variability.

In the present paper, 5 sampling events (out of 10) were selected to illustrate the evolution of chl *a*, O₂, O₂/Ar and O₂/N₂ at our location: one in the winter (BRW2 – 3 February), two in early spring (BRW4, BRW7 – corresponding to 31 March and 10 April respectively), one in mid spring (BRW8 – 8 May), and the last one in late spring (BRW10 – 5 June). The first 4 sampling events occurred during ice growth, the last one during ice decay. As mentioned in Zhou et al. (2013), BRW8 was affected by a full-depth convection event, leading to a drainage of the dissolved compounds in brine, and a partial replenishment of the dissolved compounds from seawater. This contrasted with the sampling events prior to BRW8, where convection only occurred in the permeable bottom ice layers. Finally, in BRW10, the increase of air temperature led to ice melt, full permeability and brine stratification.

2.2 Chlorophyll *a* and phaeopigment

The ice samples were melted in the dark, in 0.2 μm filtered seawater (1 : 4 volume ratio) to avoid osmotic stress. We used 10 μm and 0.8 μm polycarbonate filters in a sequence in order to distinguish larger micro-algae species from the smaller ones. Extractions and calculations were made following the procedure of Arar and Collins (1997). The standing stocks of chlorophyll *a* (chl *a*) were calculated by integrating the chl *a* concentrations over the whole ice length. The percentage of phaeopigment was obtained by dividing the concentration of phaeopigment by the sum of both chl *a* and phaeopigment concentrations. Phaeopigment results from chl *a* degradation; High percentage of phaeopigment indicates strong grazing pressure (i.e. strong impact of the respiration on the NCP).

BGD

11, 2045–2081, 2014

Insights into oxygen transport and net community production

J. Zhou et al.

Title Page

Abstract

Introduction

Conclusions

References

Tables

Figures

⏪

⏩

◀

▶

Back

Close

Full Screen / Esc

Printer-friendly Version

Interactive Discussion

2.3 O₂, Ar and N₂ concentration in ice and their respective solubility

We used the dry-crushing technique as developed for gas measurements in continental ice (Raynaud et al., 1982) to extract O₂, Ar and N₂ from the ice samples. This technique extracts both the gas bubbles in the ice and the gas in the dissolved state within liquid brine. Each ice core was cut every 5 cm, and about 60 g of sample was introduced into a vessel, with 7 stainless steel balls. The ice was crushed in the vessel, under vacuum (10⁻³ torr), as described in Stefels et al. (2012) at -25 °C. Subsequently, the vessel was kept at -50 °C in a cold ethanol bath, and was connected to the gas chromatograph equipped with a thermal conductivity detector for concentration analyses (Skoog et al., 1997). We used Alphasaz™₂ He (Air Liquide – P0252) as carrier-gas and a 22 mL packed column (Mole Sieve 5A 80/100; 5 m × 1/8"). The reproducibility of the analyses, based on triplicate analysis of five different standards, was 99.3 % for O₂, 97.8 % for Ar and 99.9 % for N₂

To determine the saturation levels of O₂, Ar and N₂ in ice and for further calculations (Sects. 2.4 and 2.5), we also determined the theoretical solubility of each gas in ice at saturation. The solubility was calculated using temperature and salinity in brine (following the relationship of Garcia and Gordon (1992) for O₂ and the relationship of Hamme and Emerson (2004) for N₂ and Ar) and the solubility was then weighted by the brine volume fraction in the ice. That weighting is necessary, as most of the impurities (including gases) are concentrated in the brine structure (and not in the pure ice matrix) (Weeks, 2010). It is noteworthy that the relationship of Hamme and Emerson (2004) was established for temperatures between 0 °C and 30 °C and for salinities between 0 and 34.5, and the relationship of Garcia and Gordon (1992) was established for temperatures between 0 and 40 °C and for salinities between 0 and 42. We thus assumed in our calculations of gas solubility that those relationships still hold for the range of temperature and salinity found in our brine samples.

BGD

11, 2045–2081, 2014

Insights into oxygen transport and net community production

J. Zhou et al.

Title Page

Abstract

Introduction

Conclusions

References

Tables

Figures

⏪

⏩

◀

▶

Back

Close

Full Screen / Esc

Printer-friendly Version

Interactive Discussion

Gas saturation levels is described following Craig and Hayward (1987) in seawater as

$$\Delta C_i = \frac{C_i}{C_{\text{eq}}} - 1. \quad (1)$$

5 where C_i is the measured concentration of the gas i in bulk ice and C_{eq} the solubility of gas i in bulk ice at equilibrium with the atmosphere, calculated at in situ temperature, salinity and pressure as described above.

2.4 O₂/Ar and O₂/N₂

10 The use of O₂/Ar and O₂/N₂ is only valid if both Ar and N₂ are inert. Ar is a noble gas, i.e., inert and not affected by any biogeochemical processes. Denitrification was found to occur in sea ice (Rysgaard et al., 2008) and could affect N₂, but we assumed that N₂ is also inert to biogeochemical processes in the present study, because N₂ is correlated to Ar with a r^2 of 0.98 (Fig. 2). Hence, both N₂ and Ar can be used as tracers for physical processes.

15 O₂/Ar and O₂/N₂ ratios were calculated from the concentrations of O₂, Ar and N₂ in ice, and were compared with their respective ratios in seawater and the atmosphere. The relative solubility of O₂/Ar in seawater (at 0 °C, with 32 of salinity) is 20.48 (Garcia and Gordon, 1992; Hamme and Emerson, 2004). However, even in abiotic conditions, the gas ratios in sea ice at initial incorporation may differ from that in seawater due to diffusion process at the ice/seawater interface (Killawee et al., 1998; Tison et al., 2002).
20 We thus applied the relative diffusion coefficient of O₂ and Ar (1.2/0.8 = 1.5) (Broecker and Peng, 1982) to our relative solubility of O₂/Ar to obtain a value of O₂/Ar with maximized diffusion processes at the bottom of sea ice (13.65) as described below. Note that different diffusion coefficients exist in the literature (Table 1) for temperature close to 0 °C or below, for seawater, water or ice; we chose to use the diffusion coefficients of
25 Broecker and Peng (1982) because it is the most recent study that provides diffusion coefficients for O₂, Ar and N₂ near the freezing temperature. Salinity is not given in

Broecker and Peng (1982), but one may expect at maximum a decrease of 4.9 % of the diffusion coefficient per increase of 35.5 of salinity (Jähne et al., 1987).

The initial values of O_2/Ar could therefore range between 13.65 and 20.48, depending on the magnitude of gas diffusion at the ice/seawater interface. Further, as O_2/Ar in the atmosphere is 22.5, gas input from the atmosphere (during frazil ice formation or when sea ice is permeable) and gas bubble formation in the permeable ice should pull the bulk ice O_2/Ar towards 22.50. Therefore, if both dissolved and gaseous states exist in the ice, O_2/Ar could range between 13.65 and 22.50, due to physical processes; that range is referred here after as the abiotic range of O_2/Ar .

We applied the same calculation to O_2/N_2 . The relative solubility in seawater is 0.56 (Garcia and Gordon, 1992; Hamme and Emerson, 2004). Since the relative diffusion coefficient between O_2 and N_2 is 1.09 (Broecker and Peng, 1982), the relative solubility with maximized diffusion processes is 0.51. Given that the atmospheric ratio of O_2/N_2 is 0.27, the abiotic range of O_2/N_2 in ice is 0.27–0.51. O_2/N_2 that is above or below this abiotic range is attributed to an impact of biological activity (Souchez et al., 2006).

2.5 NCP-related O_2 deduced from O_2/Ar

We derived the NCP-related O_2 supersaturation, $\Delta(O_2/Ar)$, also referred to as biological O_2 supersaturation and NCP-related O_2 concentrations (O_{2NCP}), using Eqs. (2) and (3) respectively, as used in seawater studies (e.g., Castro-Morales et al., 2013):

$$\Delta(O_2/Ar) = \frac{[O_2]/[Ar]}{[O_2]_{eq}/[Ar]_{eq}} - 1. \quad (2)$$

$$O_{2NCP} = [O_2]_{eq} \Delta(O_2/Ar). \quad (3)$$

in which, $[O_2]_{eq}/[Ar]_{eq}$ is the solubility ratio in seawater at equilibrium in Castro-Morales et al. (2013), but the solubility ratio in ice at equilibrium in the present study (Sect. 2.4).

In a closed system, NCP then corresponds to the changes of O_{2NCP} between sampling events. Note that in seawater studies, because of the open system, additional

BGD

11, 2045–2081, 2014

Insights into oxygen transport and net community production

J. Zhou et al.

Title Page

Abstract

Introduction

Conclusions

References

Tables

Figures

⏪

⏩

◀

▶

Back

Close

Full Screen / Esc

Printer-friendly Version

Interactive Discussion



coefficients and equations are required to take into account the diffusion at air–sea interface, the changes in the mixed layer depth and the diffusion of O_2 across the base of the mixed layer (Castro-Morales et al., 2013).

3 Results

3.1 A general overview from the standing stocks

Fig. 3 shows the standing stocks of Ar, O_2 and N_2 , in parallel with the ice thickness, for the different sampling events. N_2 reached the highest standing stocks among the three gases, followed by O_2 and then Ar. The three gas standing stocks evolved in the same way over the studied period, but not as the ice thickness: while sea ice continuously thickened from BRW2 (82 cm) to BRW10 (142 cm), the gas standing stocks increased from BRW2 to BRW8 but decreased at BRW10.

3.2 Gas saturation levels

The saturation levels of N_2 , O_2 and Ar decreased with increasing brine volume fraction (Fig. 4). The highest supersaturation of N_2 , O_2 and Ar (7030, 3180 and 2960 % respectively) corresponded to the lowest brine volume fraction (2.2 %), while the lowest undersaturations (–33, –52 and –54 % respectively) corresponded to the largest brine volume fraction (29.3 %). In addition, despite similar evolution in the standing stocks for all the gases, N_2 saturation levels contrasted with those of O_2 and Ar: N_2 reached higher supersaturation levels than O_2 and Ar, which have much similar saturation levels.

3.3 O_2 concentrations

In Fig. 5a, the dashed areas refer to the permeable ice (i.e., layers with brine volume fraction above 5 %, Golden et al., 1998). Hence, from BRW2 to BRW7, only the bottom

BGD

11, 2045–2081, 2014

Insights into oxygen transport and net community production

J. Zhou et al.

Title Page

Abstract

Introduction

Conclusions

References

Tables

Figures

⏪

⏩

◀

▶

Back

Close

Full Screen / Esc

Printer-friendly Version

Interactive Discussion



layers of the ice were permeable while at BRW8 and BRW10, the whole ice core was permeable.

Figure 5a also shows the concentration of O_2 in bulk ice ($[O_2]$, black dots) with the solubility of O_2 in ice (white dots). Mean $[O_2]$ increased from BRW2 ($67.4 \mu\text{mol L}_{\text{ice}}^{-1}$) to BRW8 ($122.4 \mu\text{mol L}_{\text{ice}}^{-1}$) and decreased at BRW10 ($93.4 \mu\text{mol L}_{\text{ice}}^{-1}$). At BRW2 and BRW4, $[O_2]$ generally exceeded the solubility of O_2 in the impermeable layers, but reached the solubility values in the permeable layers. The trends changed from BRW7 onwards: in BRW7 and BRW8, $[O_2]$ was higher than the solubility at all depths, except in the 5 last centimeters of the ice core. In BRW10, $[O_2]$ was close to the solubility of O_2 in the upper layers (from 12.5 to 72.5 cm), but exceeded the solubility of O_2 below these layers.

3.4 Chlorophyll *a* and phaeopigment concentrations

The concentrations of chl *a* [chl *a*] are reported in Zhou et al. (2013). Briefly, [chl *a*] varied largely with depth (Fig. 5b) and ranged from 0 to $83.9 \mu\text{g L}_{\text{ice}}^{-1}$ for all the sampling events. The highest [chl *a*] were always in the ice bottom, except in BRW4. Above the bottom layer, the [chl *a*] was generally below $1 \mu\text{g L}_{\text{ice}}^{-1}$. Drastic changes occurred in BRW8 when sea ice permeability increased sharply: [chl *a*] dropped at all depths, and particularly in the ice interior. [chl *a*] increased again at BRW10, showing a vertical profile and a standing stock similar to those of BRW7.

The percentage of phaeopigment also varied strongly with depth in BRW2, with over 60 % of phaeopigments in the upper ice layers but less than 20 % at the ice bottom. It varied between 20 and 40 % in BRW4 and BRW7, and increased drastically in BRW8 (with phaeopigments reaching 100 % in some layers). In BRW10, the percentage of phaeopigments varied between about 40 and 70 %, with generally the higher values in the upper ice layers.

BGD

11, 2045–2081, 2014

Insights into oxygen transport and net community production

J. Zhou et al.

Title Page

Abstract

Introduction

Conclusions

References

Tables

Figures

⏪

⏩

◀

▶

Back

Close

Full Screen / Esc

Printer-friendly Version

Interactive Discussion

3.5 O₂/Ar and O₂/N₂

O₂/Ar in ice ranged between 15.84 and 97.62 (Fig. 5c) and O₂/N₂ ranged between 0.27 and 1.47 (Fig. 5d). Both O₂/Ar and O₂/N₂ ratios are compared to their respective values in the atmosphere (22.5 and 0.27 – black and grey strait lines in Fig. 5c and d) and in seawater with maximized diffusion processes (13.65 and 0.51 – black and grey dashed lines in Fig. 5c and d).

O₂/Ar in ice at BRW2 was highly homogeneous at all depths, with a mean and standard deviation of 18.49±0.84. These ratios were found between the value of O₂/Ar in the atmosphere and that in seawater with maximized diffusion processes. Over the next sampling events, O₂/Ar in ice increased on average, exceeding the O₂/Ar in the atmosphere (the upper limit of O₂/Ar that can be explained by abiotic processes), and became more variable vertically (Fig. 5c). It is also noteworthy that from BRW4 onwards, the maximum O₂/Ar in each sampling event was found in the lower part of the ice, but never coincided with the maximum of [chl *a*], even at BRW10 where the whole profile of O₂/Ar clearly mimicked the one of [chl *a*].

The variations observed in O₂/N₂ in ice were less sensitive than those observed in O₂/Ar (Fig. 5c and d). O₂/N₂ only exceeded once the abiotic range of O₂/N₂ between BRW2 and BRW8, while O₂/Ar exceeded the abiotic range of O₂/Ar from BRW4 onwards. Similarities between O₂/Ar and O₂/N₂ were more obvious in BRW10: both ratios showed the atmospheric values at the ice surface, and they exceeded their respective abiotic range in the ice interior, with a maximum in the lower part of the ice that did not coincide with the maximum in [chl *a*].

BGD

11, 2045–2081, 2014

Insights into oxygen transport and net community production

J. Zhou et al.

Title Page

Abstract

Introduction

Conclusions

References

Tables

Figures

⏪

⏩

◀

▶

Back

Close

Full Screen / Esc

Printer-friendly Version

Interactive Discussion

4 Discussion

4.1 General dynamic of O₂ in comparison with N₂ and Ar

4.1.1 Standing stocks

To discuss the dynamics of O₂, we first compared the evolution of O₂ standing stocks against that of N₂ and Ar – two other dominant gases in sea ice that are considered to be only sensitive to physical processes in the present study (Sect. 2.4). The O₂ standing stocks that evolved in the same way as N₂ and Ar (Fig. 3) indicate that the physical controls on the O₂ standing stocks dominated over the biological ones.

Two main physical processes affect gas concentrations in ice: the incorporation during ice growth and the subsequent transport within the ice. Because of the incorporation of gases during ice growth, the gas standing stocks increased with increasing ice thickness, from BRW2 to BRW8. The decrease of gas standing stocks in BRW10, despite the fact that the ice in BRW10 was thicker than in BRW8, was then associated with subsequent transport. We attribute that subsequent transport to gas exchange through sea ice (including gas bubble escape), due to the increase of ice permeability, as discussed below.

The main evidence of gas bubble escape is the sharp decrease of gas supersaturation when the brine volume fraction exceeded 5 % (Fig. 4), hence when impermeable layers became permeable (Golden et al., 1998). Indeed, N₂ supersaturation reached up to 7000 % in the impermeable ice layers, while supersaturation of 2200 % already corresponds to gas bubble formation (Killawee et al., 1998). This observation confirms previous findings about the presence of gas bubbles in the impermeable ice layers, based on [Ar] and ice thin sections (Zhou et al., 2013). Naturally, when the impermeable ice layers became permeable, with increasing brine volume fraction, gas exchanges may occur between sea ice and the atmosphere: supersaturated gas outgassed from brine to reach the saturation level (Zhou et al., 2013), which, in turns, lowered gas standing stocks, as observed in Fig. 3.

Title Page

Abstract

Introduction

Conclusions

References

Tables

Figures

⏪

⏩

◀

▶

Back

Close

Full Screen / Esc

Printer-friendly Version

Interactive Discussion



4.1.2 Saturation levels and concentrations

Obviously, permeable sea ice allows gas exchange, but gases are not necessarily at saturation in permeable layers. Indeed, Fig. 4 shows that gases remained supersaturated for brine volume fractions above 5 % and reached 0 % or became slightly negative only for brine volume fraction exceeding 25 %. We will further discuss that relationship between O₂ saturation levels and the brine volume fraction, based on the vertical profiles of O₂ in ice (Fig. 5a).

The high O₂ supersaturations – also observed for Ar in (Zhou et al., 2013) – were associated with the upper ice layers (Fig. 5a) with brine volume fractions below 5 % (Fig. 4). We attribute this to the large accumulation of gas and the low gas solubility in those layers. Because of the temperature gradient at the beginning of ice growth, gases were incorporated in brine with higher salinity than in seawater. As a consequence, the solubility of the gases decreased, leading to gas supersaturation, and potentially gas bubble formation. When this occurs, gases preferentially accumulate in sea ice in comparison to the dissolved compounds, because gas bubbles will move upwards due to their buoyancy while dissolved compounds are subject to gravity drainage (Zhou et al., 2013). Once the ice layers became impermeable, decreasing temperature and increasing brine salinity will further decrease gas solubility in the upper layer. Both the accumulation of gas and low gas solubility induced high O₂ supersaturations in the upper ice layers with low brine volume fractions.

In contrast to the high O₂ supersaturations, O₂ undersaturations, as for N₂ and Ar, were observed in BRW10 (Fig. 5a), in the upper layers where brine volume fractions exceeded 20 % (Fig. 4). Because BRW10 was sampled during ice decay, gas bubbles have escaped from the brine due to the large brine volume fraction, and gas exchange through sea ice should allow O₂ to reach gas solubility, as for Ar (Zhou et al., 2013). Snow- and ice meltwater likely have added freshwater into brine and lowered the gas concentrations in comparison to the gas solubility. Previous analyses of water stable isotopes in brine nitrate concentrations in ice and ice texture (Zhou et al., 2013) support

BGD

11, 2045–2081, 2014

Insights into oxygen transport and net community production

J. Zhou et al.

Title Page

Abstract

Introduction

Conclusions

References

Tables

Figures

⏪

⏩

◀

▶

Back

Close

Full Screen / Esc

Printer-friendly Version

Interactive Discussion

the hypothesis of snow- and ice meltwater infiltration. The large O_2 concentrations observed in the topmost layer of BRW10 (Fig. 5a) was an exception to the general O_2 saturation and undersaturation trend, and was associated with the local development of superimposed ice layers (Zhou et al., 2013).

We qualify as moderate O_2 supersaturations those associated with ice layers where brine volume fractions exceeded 5% (Fig. 4). These permeable layers were either located in the ice bottom from BRW2 to BRW7 and throughout the ice cover in BRW8 and BRW10 (Fig. 5a). Gas solubility in these layers was higher than that in the impermeable layers, because of the higher ice temperature and lower brine salinity; the higher gas solubility lowered O_2 supersaturations, despite some local high $[O_2]$ in bulk ice (e.g., in the bottom of BRW 7 and BRW8), in comparison to the impermeable layers. Because gas exchange depends on the supersaturation levels, the observation reminds that the potential of air-ice gas exchange depends not only on the $[O_2]$ in ice, but also on the salinity and temperature-dependent solubility.

Finding moderate O_2 supersaturations in permeable layers may be counter-intuitive because permeable layers allow gas exchanges (diffusion and/or convection) that tend to remove the supersaturation. For instance, even if O_2 expulsion from growing sea ice leads to O_2 supersaturation in the ice bottom, as long as the O_2 remains in the dissolved state (Killawee et al., 1998), brine convection may replace the supersaturated O_2 with O_2 content from seawater – keeping therefore bulk O_2 close to the O_2 solubility (as observed in Fig. 5a – BRW2, BRW4, bottom third of the ice cover). Another evidence of gas exchange in permeable layer is the decrease of O_2 standing stocks and O_2 saturations in BRW10, associated with the increase of ice permeability, as demonstrated earlier. Therefore, we suggest that the moderate gas supersaturations in the permeable layers resulted from either a transition stage where gas exchange was ongoing (i.e., tending toward the saturation), and/or a net community production of O_2 (NCP) that overwhelmed the loss of O_2 through physical processes, as discussed here below.

Insights into oxygen transport and net community production

J. Zhou et al.

[Title Page](#)[Abstract](#)[Introduction](#)[Conclusions](#)[References](#)[Tables](#)[Figures](#)[⏪](#)[⏩](#)[◀](#)[▶](#)[Back](#)[Close](#)[Full Screen / Esc](#)[Printer-friendly Version](#)[Interactive Discussion](#)

Insights into oxygen transport and net community production

J. Zhou et al.

Title Page

Abstract

Introduction

Conclusions

References

Tables

Figures

⏪

⏩

◀

▶

Back

Close

Full Screen / Esc

Printer-friendly Version

Interactive Discussion

A transition stage would characterize the impermeable ice layers that became permeable, like in the upper layers of BRW8. The initial supersaturated O_2 content tended toward saturation, as observed in some upper layers of BRW10. The duration needed for gas equilibrium depends on the efficiency of the gas transport through the brine network (Loose et al., 2010).

On the top of the physical transport of O_2 during the transition stage, NCP also contributed to O_2 supersaturation in permeable layers. The most obvious evidence of NCP contribution was from the bottom layers of BRW10. O_2 supersaturations due to physical processes were unlikely during ice decay: $[Ar]$ was at saturation (or slightly undersaturated) over the whole ice length, indicating the absence of gas bubbles and the infiltration of snow- or ice meltwater (Zhou et al., 2013). The increase of $[chl\ a]$ in the bottom layers of BRW10 (Fig. 5b – BRW10) then points to a NCP-related O_2 supersaturation. Note that despite the fact that the biological O_2 supersaturation (through NCP) dominated over the physical one, it did not prevent the decrease of O_2 standing stocks between BRW8 and BRW10 (Fig. 3). Further, the maximum of $[chl\ a]$ (130–140 cm) mismatched with the maximum of $[O_2]$ (125–130 cm), which is unexpected if the O_2 supersaturation was NCP-related. Because of the constant phaeopigment percentage in those bottom layers (i.e., potentially constant algal degradation), precluding difference in net community productivity (NCP/ $chl\ a$ ratio), we attribute the decrease of $[O_2]$, from 125 cm to the interface, to the diffusion of the NCP-related O_2 from sea ice to seawater. Similar decrease of bulk O_2 concentrations in the 20 last cm of sea ice, in BRW7 and BRW8, may also depict the combined effect of NCP and O_2 transport.

4.2 O_2/Ar and O_2/N_2 : sensitivity and ability to assess the biological contribution to O_2 dynamics

Because both NCP and physical processes (dilution, transport) affected the $[O_2]$ in sea ice, we need to remove the physical contribution to determine the NCP-related O_2 in sea ice. Comparing the variation of O_2 against that of an inert gas (that is solely dependent on physical processes) allows to decipher the variation of O_2 related to NCP.

Insights into oxygen transport and net community production

J. Zhou et al.

Title Page

Abstract

Introduction

Conclusions

References

Tables

Figures

⏪

⏩

◀

▶

Back

Close

Full Screen / Esc

Printer-friendly Version

Interactive Discussion

Recent studies have indeed used O_2/Ar to remove the physical contribution and to determine NCP in seawater (Cassar et al., 2009; Castro-Morales et al., 2013; Hendricks et al., 2004; Reuer et al., 2007), while O_2/N_2 was shown to be sensitive to the biological activity in basal continental ice (e.g., Souchez et al., 2006). In this section, we will discuss the behavior of both O_2/Ar and O_2/N_2 ratios, and discuss on the feasibility to use them for determining NCP in sea ice.

4.2.1 General trends of O_2/N_2 and O_2/Ar

The range of O_2/N_2 from BRW2 to BRW7 (0.27 and 0.41) remained within the abiotic range (0.27–0.51), hence the observed variations of O_2 against N_2 was not strong enough to preclude the possibility that these were solely associated with physical processes. Indeed, the observed range is consistent with those obtained from ice growth experiments in abiotic conditions (0.37–0.45) (Killawee et al., 1998), or with negligible bacteria activities (0.32–0.44) (Tison et al., 2002). In contrast, the increase of O_2/N_2 up to 1.47, i.e., beyond the abiotic range, in BRW10, indicates that the contribution of NCP to the $[O_2]$ dominates over that of the physical processes. Therefore, the evolution of O_2/N_2 indicated a transition from a physical-dominated O_2 supersaturation (from BRW2 to BRW8) to a NCP-dominated O_2 supersaturation (in BRW10). This is in agreement with what we observed from gas standing stocks, gas saturation levels and brine volume fraction (Sect. 4.1).

From the best of our knowledge, O_2/Ar has never been measured in ice before; a comparison with the literature is therefore impossible. However, since O_2/Ar and O_2/N_2 evolve similarly toward higher values over the sampling events, sharp increase in O_2/Ar likely indicate, as O_2/N_2 , the switch from physical-dominated to NCP-dominated O_2 supersaturation.

4.2.2 Comparison of the sensitivity of O₂/N₂ and O₂/Ar

The main difference between O₂/Ar and O₂/N₂ (Fig. 5c and d) was their variability with depth: O₂/Ar appeared more sensitive than O₂/N₂ to describe the NCP-related O₂ supersaturation, because it exceeded the abiotic range from BRW4 onwards (vs. BRW8 for O₂/N₂). That difference may result from (1) the relative abundance of O₂ compared to those of Ar and N₂, (2) the relative solubilities of the gases and (3) the relative diffusion rates of the gases. First, since [O₂] is about 20 times higher than [Ar], but about 3 times lower than [N₂], adding the same amount of O₂ (due to NCP) will induce a higher increase in the O₂/Ar ratio than in the O₂/N₂ ratio. Second, N₂ solubility in brine was clearly different to that of O₂ and Ar, as suggested by the larger supersaturation of N₂ in comparison to O₂ and Ar (Fig. 4). That difference in gas solubility impacts the fractionation between gases in brine and gas bubbles, which then affect differently the O₂/Ar and O₂/N₂ ratios. Third, the diffusion coefficient in seawater of O₂, Ar, and N₂ are 1.2, 0.8 and 1.1 (10⁻¹⁵ cm² s⁻¹) respectively (Broecker and Peng, 1982). If diffusion occurs in the permeable bottom ice layers (Killawee et al., 1998), both O₂/Ar and O₂/N₂ ratios will decrease: O₂/Ar by a factor 1.5, but O₂/N₂ only by a factor 1.1.

We made a simple calculation to assess the impact of maximized gas bubble formation and diffusion on O₂/Ar and O₂/N₂. Gas bubble formation will draw O₂/Ar from 20.48 (solubility in seawater) to 22.5 (ratio in gas bubbles) (see materials and methods), resulting in an increase of O₂/Ar by 9.9%. Gas diffusion privileges the loss of O₂ in comparison to Ar, with a ratio of 1.2/0.8 due to their respective diffusion coefficient (Broecker and Peng, 1982), resulting in a decrease of O₂/Ar from 20.48 to 13.65, i.e., -33.3%. When we applied the same calculations to O₂/N₂, assuming O₂/N₂ ratios of 0.56 in seawater, 0.27 in gas bubbles and a relative coefficient of 1.1, we obtained a change of O₂/N₂ by -51.8% due to gas bubble formation and -8.9% due to diffusion. Therefore, maximizing both physical processes will decrease O₂/Ar by 23.4%, but O₂/N₂ by 60.7%.

Surprisingly, the NCP that was derived from O₂ standing stocks (NCP(O₂)) differed significantly from the NCP derived from O₂/Ar (NCP(O₂/Ar)) and varied much largely with depth (Table 3). We attribute this to the spatial variability of gases because extreme values of NCP(O₂) were observed at 20–40 cm depth, where bulk O₂ changed abruptly in BRW4 (Fig. 5a). It is unclear for us why [O₂] varied in this way in BRW4, but Ar showed the same trend (Zhou et al., 2013), precluding therefore drastic O₂ changes associated with NCP; the deduced NCP(O₂) was then likely an artifact of the spatial variability in BRW4. In that situation, the correction of O₂ using Ar, which was incorporated in the same conditions than O₂ (i.e., experiencing the same spatial variability) would correct the effect of spatial variability on NCP.

However, another cause of the differences between NCP(O₂) and NCP(O₂/Ar) may be the values of [O₂]_{eq} prescribed in the calculation of NCP(O₂/Ar) (Eq. 3). In seawater studies, the NCP-related O₂ concentration is defined as [O₂]_{eq}Δ(O₂/Ar) (Eq. 3), where [O₂]_{eq} is the temperature and salinity-dependent O₂ solubility in ice. In our impermeable sea ice layers, the initial O₂ concentration may be supersaturated, i.e., higher than the gas solubility calculated at in situ temperature and salinity following Garcia and Gordon (1992) ([O₂]_{eq}), because of the various processes described in Sect. 4.1.2. Indeed, Ar supersaturation approached 500 % for brine volume fraction of 5 % (the transition from permeable to impermeable layers) (Fig. 4) – in comparison to the 1 % of supersaturation reported in seawater studies (Hamme and Severinghaus, 2007), but 564 % in Antarctic lake ice (Hood et al., 1998) – indicating that the initial O₂ concentration, from which we can start to correct the physical processes using O₂/Ar, may be supersaturated as well: at least 500 % if we assumed similar solubility between O₂/Ar (Weiss, 1970), and even more if we take into account the O₂ production in the bottom ice layers.

Clearly, both O₂-based and O₂/Ar-based techniques to derive NCP in impermeable layers have their limitations. We multiplied the NCP(O₂/Ar) by 5 and by 30 to take into account the full range of O₂ supersaturation when the ice became impermeable (Fig. 4). Corrected NCP(O₂/Ar) then ranged between 5.0 and 81.4 (10⁻³ mmol O₂ m⁻² d⁻¹) from BRW2 to BRW4, and between -333.6 and 356.4

BGD

11, 2045–2081, 2014

Insights into oxygen transport and net community production

J. Zhou et al.

Title Page

Abstract

Introduction

Conclusions

References

Tables

Figures

⏪

⏩

◀

▶

Back

Close

Full Screen / Esc

Printer-friendly Version

Interactive Discussion

($10^{-3} \text{ mmol O}_2 \text{ m}^{-2} \text{ d}^{-1}$) from BRW4 to BRW7. These values are very modest compared to the NCP reported in springtime sea ice bottom in Greenland (Long et al., 2012) and in the Barents sea (McMinn and Hegseth, 2007) (-1.45 and $3.1 \text{ mmol O}_2 \text{ m}^{-2} \text{ d}^{-1}$ respectively, assuming a O_2/C ratio of 1.43 following Glud et al., 2002), but one has to consider that surface ice layers are likely much less productive than the permeable sea ice bottom.

The observed fluctuations of $\text{NCP}(\text{O}_2/\text{Ar})$ from BRW4 to BRW7 witness that heterotrophic and autotrophic processes may coexist in sea ice. This is not surprising because the presence of micro-niches allow both processes to coexist in sea ice (Rysgaard et al., 2008). The change from net autotrophic (BRW2-BRW4) to both autotrophic and heterotrophic system (BRW4-BRW7) is in agreement with the results of previous analyses suggesting increasing remineralisation (i.e., net heterotrophic processes) in BRW7 (Zhou et al., 2013).

4.3.2 The permeable layers

For the permeable layers, O_2 exchanges through sea ice were obvious (Sect. 4.1). As a consequence, changes in O_2 standing stocks do not allow retrieving NCP. O_2/Ar was clearly sensitive to NCP, but requires additional equations that describe gas bubble formation and gas diffusion to remove the physical imprints in O_2/Ar . As we could not assess the frequency or the impact of the convection on the variations of O_2 over the sampling period, we simplified the problem by considering only the case of BRW10 where convection was unlikely due to brine stratification (Sect. 2.1) (i.e., only diffusion and NCP took place). At that time, sea ice was completely permeable and physical O_2 supersaturation should be inexistent (Sect. 4.1), the technique of O_2/Ar should then be applicable as in seawater.

We described the variation of $[\text{O}_2]$ at a depth z , over a period of time t ($\frac{\partial[\text{O}_2]_z}{\partial t}$), as a function of the net community production at the depth z (NCP_z) and the diffusion of O_2 between that depth (z) and the layers above ($z - 1$) and below ($z + 1$). The diffusion

BGD

11, 2045–2081, 2014

Insights into oxygen transport and net community production

J. Zhou et al.

Title Page

Abstract

Introduction

Conclusions

References

Tables

Figures

⏪

⏩

◀

▶

Back

Close

Full Screen / Esc

Printer-friendly Version

Interactive Discussion

itself depends on the concentration gradient, and DO_2 which is set as the molecular diffusion coefficient of O_2 in seawater at $0^\circ C$, $1.2 \times 10^{-5} cm^2 s^{-1}$ (Broecker and Peng, 1982). There is an error ϕ due to the impact of physical processes on O_2 . This gives:

$$\frac{\partial [O_2]_z}{\partial t} = D_{O_2} \frac{\partial O_2}{\partial z^2} + NCP_z + \phi \quad (4)$$

Assuming a steady state (i.e, all the new O_2 production due to NCP diffused away so that the profile of BRW10 (Fig. 5a) remained constant), and assuming that O_2/Ar corrects the changes of O_2 changes due to solubility changes as in seawater (Weiss, 1970), Eq. 4 can be approximate as

$$NCP_z = -D_{O_2} \frac{\partial^2 ([O_2]_{eq} \Delta(O_2/Ar))}{\partial z^2} \quad (5)$$

could neither retrieve the NCP_z in the last 5 cm of the ice bottom, as the calculation of NCP_z of a layer depends on the adjacent layers, nor the NCP_z in the surperimposed ice at the top of the ice cover as temperature and salinity data were missing. It is also noteworthy that this calculation is sensitive to the diffusion coefficient, which is highly variable (Table 1): using the O_2 diffusion coefficient of Loose et al. (2010) instead of that of Broecker and Peng (1982) will triple the estimate of NCP. Discussing the causes of the variability in O_2 diffusion coefficient is beyond the scope of the present paper. Instead, we simply used the coefficients from Broecker and Peng (1982) to provide a conservative estimate of NCP.

Figure 6 shows the results of NCP_z , hence the deduced NCP at different depth assuming a steady state, where diffusion equals the NCP. NCP_z varied vertically, but the sharp increase of NCP_z at 125–130 cm clearly stood out, corresponding to an O_2 production of $51 mmol O_2 m^{-2} d^{-1}$, hence a C uptake of $435 mg C m^{-2} d^{-1}$. The smaller variations in the deduced NCP_z may reflect the spatial heterogeneity of the system (Sect. 4.3.1) or a numerical effect, because the use of second derivatives implies strong

sensitivity to the gradient of concentrations. For example, the negative C uptake at 115–120 cm depth (Fig. 6) may be related to a sharp change of NCP (also noticeable in the profiles of O₂, Fig. 3a). Therefore, we suggest a conservative interpretation of the NCP based on the integration of NCP_z over some layers or over the whole ice length, which also facilitate the comparison with previous data. The integration gives as NCP –0.12, 23.52 and 23.51 mmolO₂m⁻²d⁻¹ in the top 50 cm layer, bottom 20 cm and in the whole ice cover respectively.

The negative NCP in the top 50 cm layers indicates net heterotrophy, hence a C release of 1.0 mgCm⁻²d⁻¹ (assuming the photosynthetic quotient O₂/C of 1.43, Glud et al., 2002). The NCP in the bottom permeable layers (23.52 mmolO₂m⁻²d⁻¹) contributed to a large part of the NCP over the whole ice length (23.51 mmolO₂m⁻²d⁻¹), which is not surprising because chl *a* was mainly concentrated at the sea ice bottom. Comparison with the previous data in the literature is difficult because of the vertical resolution of the analyses. For instance, our equivalent C uptake in the bottom layer (197.3 mgCm⁻²d⁻¹) is much larger than the 84.2 mgCm⁻²d⁻¹ observed in Barrow landfast sea ice bottom (Lee et al., 2008) the 27 May 2003, but considering that we integrated the O₂ production over 20 cm of ice layer vs. the 3-bottommost-cm ice layer in Lee et al. (2008), we may expect higher deduced NCP. Therefore, we will only highlight that we are confident about our estimate of NCP, as it is within the range of primary production in the springtime bottom sea ice of the Canadian Arctic Archipelago (21–463 mgCm⁻²d⁻¹) (Smith et al., 1988) and Baffin Bay (26–317 mgCm⁻²d⁻¹) (Nozais et al., 2001).

The deduced C uptake over the whole ice length (197.3 mgCm⁻²d⁻¹) was 10 times higher than the maximum C uptake of 12 mgCm⁻²d⁻¹ from the atmosphere (Nomura et al., 2010). Given to the variation of C uptake with depth (C release in the upper layers and C uptake in the bottom layer), we believe that the under-ice water was the main source of C supply for sea ice.

5 Conclusion and perspectives

We presented the evolution of O_2 standing stocks, saturation levels and concentrations in landfast sea ice, collected in Barrow (Alaska) from February to June 2009. The comparison of the standing stocks and saturations levels of O_2 with those of N_2 and Ar reveals that the dynamic of O_2 in sea ice was highly sensitive to physical processes. Ice growth and gas bubble formation had favored the incorporation of O_2 in sea ice, and low brine volume fraction (i.e., low permeability) maintained high supersaturation of O_2 in sea ice. Increasing ice permeability during ice melt led to gas exchange through sea ice, which lowered the O_2 standing stocks, despite significant net biological O_2 production (NCP). Because of gas exchange through sea ice (i.e., with seawater and the atmosphere), understanding the variations of O_2 and NCP with depth in sea ice is highly complementary to the eddy-correlation technique that measures NCP at the ice–water interface; it should highlight the proportion of O_2 transferred from sea ice to seawater and the proportion that is transferred from sea ice to the atmosphere (respectively measured and neglected in the eddy-correlation technique).

O_2 exchange through sea ice depends not only on ice permeability (i.e., brine volume fraction), but also on O_2 solubility. While increasing temperature increases ice permeability, which allows gas exchanges, it also increases O_2 solubility (through decreasing brine salinity). As a consequence, although high O_2 supersaturations were found in impermeable layers, the potential for gas exchanges decreased as sea ice became permeable. That relationship between saturation levels and brine volume fraction also implies that gas exchange may be intense in winter (low ice temperature) on mechanically-weakened sea ice covers. Further analyses in ice ridging areas should confirm that conjecture.

Because O_2 was mainly sensitive to physical processes, we tested the use of O_2/Ar and O_2/N_2 to correct for the physical contribution and to determine the net biological contribution to O_2 variations (i.e., NCP). O_2/Ar suited better than O_2/N_2 for NCP determination, because the relative abundance of O_2 , N_2 and Ar induced higher sensitivity in

BGD

11, 2045–2081, 2014

Insights into oxygen transport and net community production

J. Zhou et al.

Title Page

Abstract

Introduction

Conclusions

References

Tables

Figures

⏪

⏩

◀

▶

Back

Close

Full Screen / Esc

Printer-friendly Version

Interactive Discussion

O₂/Ar, and the combined effect of maximized gas bubble formation and gas diffusion induced less bias in O₂/Ar. Further, O₂/Ar showed the ability to correct for the impact of spatial variability on the determination of NCP based on O₂ solely, as both O₂ and Ar were incorporated in the same physical conditions (i.e., subject to the same spatial variability).

We estimated conservative NCP in the impermeable layers of sea ice. These are the first estimates derived from O₂ measurements in sea ice, because the technique of crushing allows measurements in the impermeable layers. However, the estimates were only conservative, because of uncertainties related to O₂ concentrations (and potential supersaturation) at bubble close-off. Further work that deals with gas solubility for temperature and salinity in brine may solve this issue and provide more accurate NCP estimate in the impermeable layers.

We also derived NCP using the O₂/Ar technique for the permeable layers (BRW10). The results suggest heterotrophic conditions in the upper ice layers, but autotrophic conditions at sea ice bottom – which contributed to most of the total NCP of the whole ice cover. Because O₂ and C are tightly-related in photosynthetic and respiration processes, the vertical profile of NCP indicates C release to the atmosphere in the upper layers, but C uptake in the bottom ice layers, where seawater was likely the main source of C supply.

Acknowledgements. The authors would like to thank Hajo Eicken, the rest of the sea ice group of the Geophysical Institute of the University of Alaska Fairbanks, Nicolas-Xavier Geilfus, Gauthier Carnat, Tim Papakyriakou, Bernard Heinesch, Michel Yernaux, Thomas Goossens, Noémie Carnat and Rodd Laing for their help in field work. We are indebted to the Barrow Arctic Science Consortium and the North Slope Borough for their logistical support. We also thank Saïda El Amri for her efficient help in laboratory work, Neige Egmont for her comments and Roberta Hamme for sharing the matlab script on gas diffusion. This research was supported by the F.R.S-FNRS (contract 2.4584.09), the National Science Foundation (project OPP-0632398 (SIZONet)), the University of Alaska Fairbanks and the Belgian Science Policy (contract SD/CA/03A), the NCE ArcticNet and National Science and Engineering Research Council

Insights into oxygen transport and net community production

J. Zhou et al.

[Title Page](#)[Abstract](#)[Introduction](#)[Conclusions](#)[References](#)[Tables](#)[Figures](#)[Back](#)[Close](#)[Full Screen / Esc](#)[Printer-friendly Version](#)[Interactive Discussion](#)

(NSERC). FB was a research fellow of F.R.S.-FRIA, JZ a research fellow of F.R.S.-FNRS, and BD, a research associate of F.R.S.-FNRS. This is MARE contribution no. XXX.

References

5 Arar, E. J. and Collins, G. B.: In vitro Determination of Chlorophyll *a* and Pheophytin *a* in Marine and Freshwater Algae by Fluorescence (Method 445.0), National Exposure Research Laboratory – US Environmental Protection Agency, Ohio, 1997.

Arrigo, K. R., Mock, T., and Lizotte, M. P.: Primary producers and sea ice, in: Sea Ice, edited by: Thomas, D. N. and Dieckmann, G. S., Blackwell Publishing Ltd, UK, 2010.

10 Brierley, A. S. and Thomas, D. N.: Ecology of Southern Ocean pack ice, *Adv. Mar. Biol.*, 43, 171–276, 2002.

Broecker, W. S. and Peng, T. H.: Gas exchange rates between air and sea, *Tellus*, 26, 21–35, 1974.

Broecker, W. S. and Peng, T.: Tracers in the Sea, The Lamont-Doherty Geological Observatory, Columbia University, New York, 1982.

15 Cassar, N., Barnett, B., Bender, M. L., Kaiser, J., Hamme, R. C., and Tilbrook, B.: Continuous high-frequency dissolved O₂/Ar measurements by Equilibrator Inlet Mass Spectrometry (EIMS), *Anal. Chem.*, 81, 1855–1864, 2009.

Castro-Morales, K., Cassar, N., Shoosmith, D. R., and Kaiser, J.: Biological production in the Bellingshausen Sea from oxygen-to-argon ratios and oxygen triple isotopes, *Biogeosciences*, 10, 2273–2291, doi:10.5194/bg-10-2273-2013, 2013.

20 Craig, H. and Hayward, T.: Oxygen supersaturation in the ocean: biological versus physical contributions, *Science*, 235, 199–202, 1987.

Garcia, H. E. and Gordon, L. I.: Oxygen solubility in seawater: better fitting equations, *Limnol. Oceanogr.*, 37, 1307–1312, 1992.

25 Glud, R. N., Rysgaard, S., and Kuhl, M.: A laboratory study on O₂ dynamics and photosynthesis in ice algal communities: quantification by microsensors, O₂ exchange rates, C-14 incubations and a PAM fluorometer, *Aquat. Microb. Ecol.*, 27, 301–311, 2002.

Golden, K. M., Ackley, S. F., and Lytle, V. I.: The percolation phase transition in sea ice, *Science*, 282, 2238–2241, 1998.

BGD

11, 2045–2081, 2014

Insights into oxygen transport and net community production

J. Zhou et al.

Title Page

Abstract

Introduction

Conclusions

References

Tables

Figures

⏪

⏩

◀

▶

Back

Close

Full Screen / Esc

Printer-friendly Version

Interactive Discussion

Insights into oxygen transport and net community production

J. Zhou et al.

[Title Page](#)

[Abstract](#)

[Introduction](#)

[Conclusions](#)

[References](#)

[Tables](#)

[Figures](#)

[⏪](#)

[⏩](#)

[◀](#)

[▶](#)

[Back](#)

[Close](#)

[Full Screen / Esc](#)

[Printer-friendly Version](#)

[Interactive Discussion](#)



Nomura, D., Eicken, H., Gradinger, R., and Shirasawa, K.: Rapid physically driven inversion of the air–sea ice CO₂ flux in the seasonal landfast ice off Barrow, Alaska after onset of surface melt, *Cont. Shelf Res.*, 30, 1998–2004, 2010.

Nozais, C., Gosselin, M., Michel, C., and Tita, G.: Abundance, biomass, composition and grazing impact of the sea ice meiofauna in the North Water, northern Baffin Bay, *Mar. Ecol.-Prog. Ser.*, 217, 235–250, 2001.

Raynaud, D., Delmas, R., Ascencio, J. M., and Legrand, M.: Gas extraction from polar ice cores: a critical issue for studying the evolution of atmospheric CO₂ and ice-sheet surface elevation, *Ann. Glaciol.*, 3, 265–268, 1982.

Reuer, M. K., Barnett, B. A., Bender, M. L., Falkowski, P. G., and Hendricks, M. B.: New estimates of Southern Ocean biological production rates from O₂/Ar ratios and the triple isotope composition of O₂, *Deep-Sea Res. Pt. I*, 54, 951–974, 2007.

Rysgaard, S., Glud, R. N., Sejr, M. K., M. E., Blicher, B., and Stahl, H. J.: Denitrification activity and oxygen dynamics in Arctic sea ice, *Polar Biol.*, 31, 527–537, 2008.

Skoog, D. A., West, D. M., and Holler, F. J.: *Chimie Analytique*, De Boeck Université, Paris, Bruxelles, 1997.

Smith, R. E. H., Anning, J., Clement, P., and Cota, G. F.: Abundance and production of ice algae in Resolute Passage, Canadian Arctic, *Mar. Ecol.-Prog. Ser.*, 48, 251–263, 1988.

Souchez, R., Jouzel, J., Landais, A., Chappellaz, J., Lorrain, R., and Tison, J. L.: Gas isotopes in ice reveal a vegetated central Greenland during ice sheet invasion, *Geophys. Res. Lett.*, 33, L24503, doi:10.1029/2006gl028424, 2006.

Stefels, J., Carnat, G., Dacey, J. W. H., Goossens, T., Elzenga, J. T. M., and Tison, J. L.: The analysis of dimethylsulfide and dimethylsulfoniopropionate in sea ice: dry-crushing and melting using stable isotope additions, *Mar. Chem.*, 128–129, 34–43, 2012.

Thomas, D. N. and Dieckmann, G. S.: Antarctic sea ice—a habitat for extremophiles, *Science*, 295, 641–644, 2002.

Tison, J. L., Haas, C., Gowing, M. M., Sleewagen, S., and Bernard, A.: Tank study of physico-chemical controls on gas content and composition during growth of young sea-ice, *J. Glaciol.*, 48, 267–278, 2002.

Vancoppenolle, M., Meiners, K. M., Michel, C., Bopp, L., Brabant, F., Carnat, G., Delille, B., Lannuzel, D., Madec, G., Moreau, S., Tison, J.-L., and van der Merwe, P.: Role of sea ice in global biogeochemical cycles: emerging views and challenges, *Quaternary Sci. Rev.*, 79, 207–230, 2013.

Weeks, W. F.: On Sea Ice, University of Alaska Press, Alaska, 2010.

Weiss, R. F.: The solubility of nitrogen, oxygen and argon in water and seawater, Deep Sea Res., 17, 721–735, 1970.

5 Zhou, J., Delille, B., Eicken, H., Vancoppenolle, M., Brabant, F., Carnat, G., Geilfus, N.-X., Papakyriakou, T., Heinesch, B., and Tison, J.-L.: Physical and biogeochemical properties in landfast sea ice (Barrow, Alaska): insights on brine and gas dynamics across seasons, J. Geophys. Res.-Oceans, 118, 3172–3189, 2013.

BGD

11, 2045–2081, 2014

Insights into oxygen transport and net community production

J. Zhou et al.

Title Page

Abstract

Introduction

Conclusions

References

Tables

Figures



Back

Close

Full Screen / Esc

Printer-friendly Version

Interactive Discussion



Insights into oxygen transport and net community production

J. Zhou et al.

Table 1. Diffusion coefficients of O₂, Ar and N₂ found in the literature for different medium (water, seawater and sea ice) for temperature at or below 0 °C. Salinity is given when available. The diffusion coefficients in use in the present study are those of Broecker and Peng (1982).

	Medium	Temperature °C	Salinity	O ₂ 10 ⁻⁵ cm ² s ⁻¹	Ar 10 ⁻⁵ cm ² s ⁻¹	N ₂ 10 ⁻⁵ cm ² s ⁻¹
Broecker and Peng (1974)	Water	0	–	1.17	0.88	0.95
Broecker and Peng (1982)	Seawater	0	–	1.2	0.8	1.1
Loose et al. (2010)	Ice	–12 to –4	3.78–6.58	3.9	–	–

Title Page

Abstract

Introduction

Conclusions

References

Tables

Figures

⏪

⏩

◀

▶

Back

Close

Full Screen / Esc

Printer-friendly Version

Interactive Discussion



Insights into oxygen transport and net community production

J. Zhou et al.

[Title Page](#)

[Abstract](#)

[Introduction](#)

[Conclusions](#)

[References](#)

[Tables](#)

[Figures](#)



[Back](#)

[Close](#)

[Full Screen / Esc](#)

[Printer-friendly Version](#)

[Interactive Discussion](#)

Table 2. Synthesis on the trends of changes of O_2/Ar and O_2/N_2 at the ice–water interface. An upward arrow indicates that the process increases the ratio, while a downward arrow indicates that the process decreases the ratio. The percentages in brackets indicate the maximal changes of the ratio associated with the physical processes (see Sect. 4.2.2 for details).

	O_2/Ar	O_2/N_2
Photosynthesis	↑	↑
Respiration	↓	↓
Gas bubble formation	↑ (+9.9%)	↓ (−51.8%)
Diffusion	↓ (−33.3%)	↓ (−8.9%)

Insights into oxygen transport and net community production

J. Zhou et al.

Table 3. NCP in the impermeable ice layers (0–50 cm depth) from BRW2 to BRW4 and from BRW4 to BRW7, in $\text{mmol O}_2 \text{m}^{-2} \text{d}^{-1}$. The columns entitled “O₂meth.” refer to the NCP derived from the standing stocks of [O₂] in bulk ice, while the columns entitled “O₂/Ar” refer to the NCP derived using the O₂/Ar (see Eqs. 2 and 3).

Ice depth (cm)	BRW2-BRW4		BRW4-BRW7	
	O ₂ meth.	O ₂ /Ar meth.	O ₂ meth.	O ₂ /Ar meth.
0–10	–6.9	1.0	–124.1	11.9
10–20	–1.0	1.1	–378.8	–3.8
20–30	–76.9	1.4	488.7	3.4
30–40	106.9	2.1	–661.1	–11.1
40–50	33.2	2.7	–387.2	–11.0

Title Page

Abstract

Introduction

Conclusions

References

Tables

Figures

⏪

⏩

◀

▶

Back

Close

Full Screen / Esc

Printer-friendly Version

Interactive Discussion

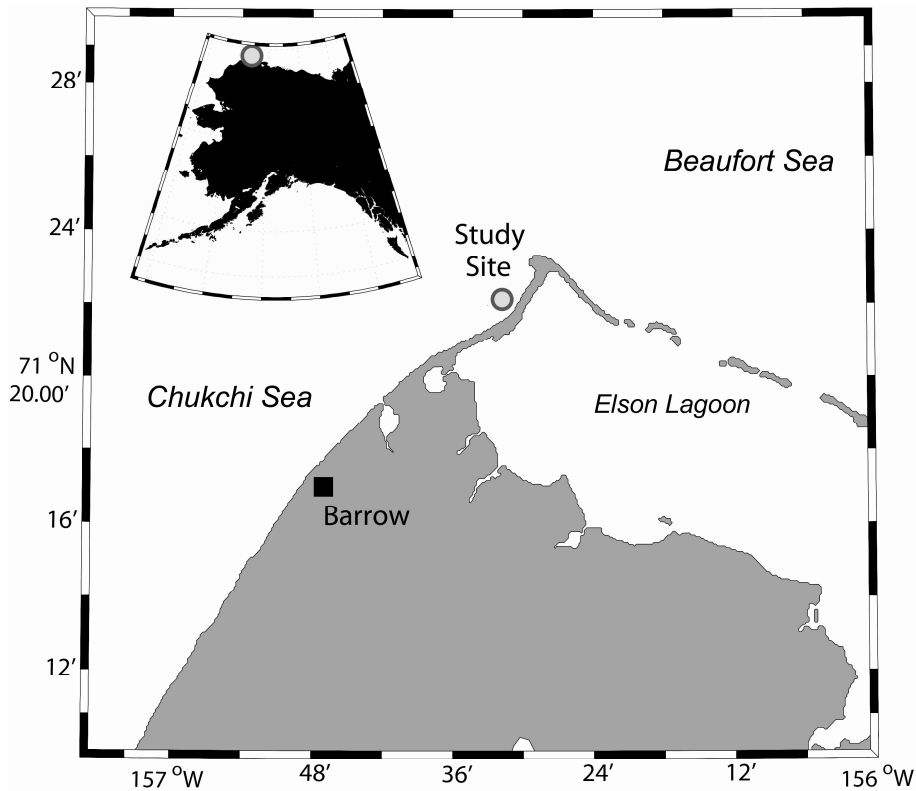


Fig. 1. The study site, North of Barrow (Alaska, USA).

Insights into oxygen transport and net community production

J. Zhou et al.

Title Page	
Abstract	Introduction
Conclusions	References
Tables	Figures
◀	▶
◀	▶
Back	Close
Full Screen / Esc	
Printer-friendly Version	
Interactive Discussion	



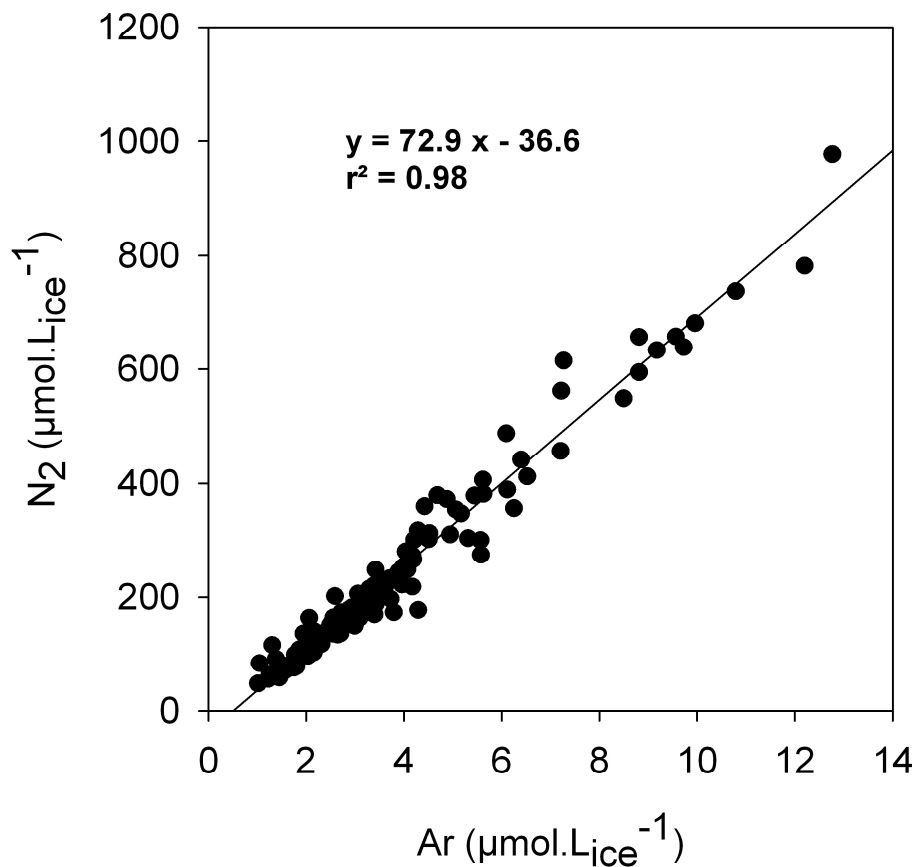


Fig. 2. Concentrations of N₂ in ice plotted against the concentrations of Ar in ice. The equation and r^2 are calculated assuming a linear regression between both gas concentrations.

Insights into oxygen transport and net community production

J. Zhou et al.

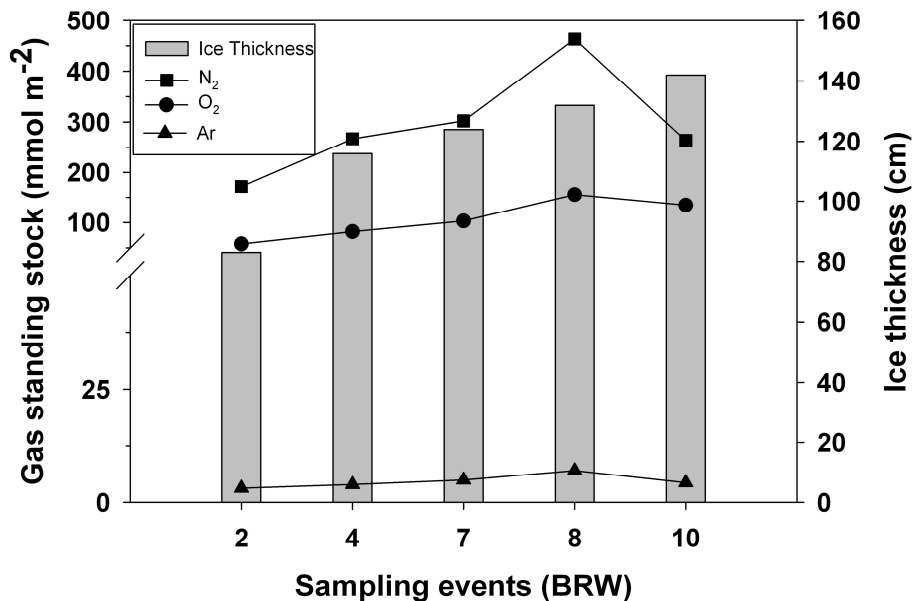


Fig. 3. Evolution of the standings stocks of N₂, O₂ and Ar (squares, circles and triangles respectively) compared to the evolution of sea ice thickness (vertical grey bars). The break in gas standing stocks is set at 50 mmol m⁻².

Title Page

Abstract

Introduction

Conclusions

References

Tables

Figures

◀

▶

◀

▶

Back

Close

Full Screen / Esc

Printer-friendly Version

Interactive Discussion

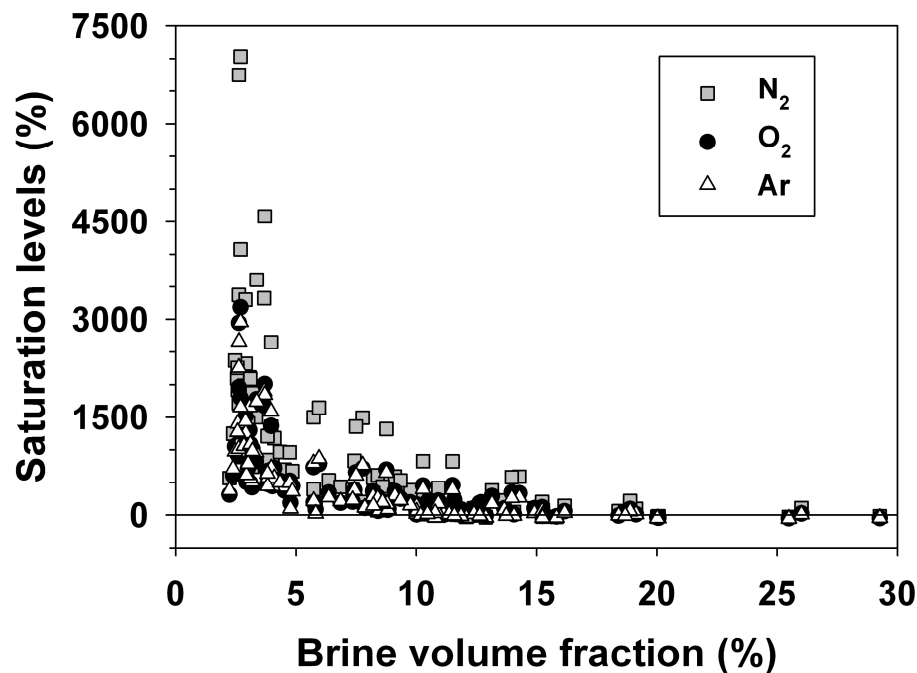


Fig. 4. Saturation levels (ΔC_i in Eq. (1), in percentage) of N₂, O₂ and Ar (squares, circles and triangles respectively) compared to the brine volume fraction.

[Title Page](#)[Abstract](#)[Introduction](#)[Conclusions](#)[References](#)[Tables](#)[Figures](#)[⏪](#)[⏩](#)[◀](#)[▶](#)[Back](#)[Close](#)[Full Screen / Esc](#)[Printer-friendly Version](#)[Interactive Discussion](#)

Insights into oxygen transport and net community production

J. Zhou et al.

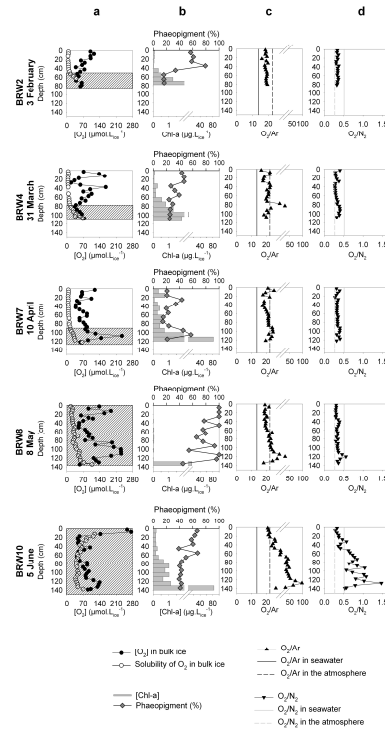


Fig. 5. (a) O_2 concentration in bulk ice (black dots) compared to its solubility in ice (white dots), the dashed areas refer to permeable ice layers (i.e. with a brine volume fraction above 5%); (b) Chl *a* concentrations (horizontal bars) with a break at $2 \mu\text{g L}_{\text{ice}}^{-1}$ compared to the percentage of phaeopigments (diamonds); (c) O_2/Ar in ice (upside triangles) with a break at 25, compared to the same ratios in seawater (straight black line) and in the atmosphere (dashed black line); (d) O_2/N_2 in ice (downside triangles) compared the same ratios in seawater (straight grey line) and in the atmosphere (dashed grey line).

Title Page

Abstract

Introduction

Conclusions

References

Tables

Figures



Back

Close

Full Screen / Esc

Printer-friendly Version

Interactive Discussion

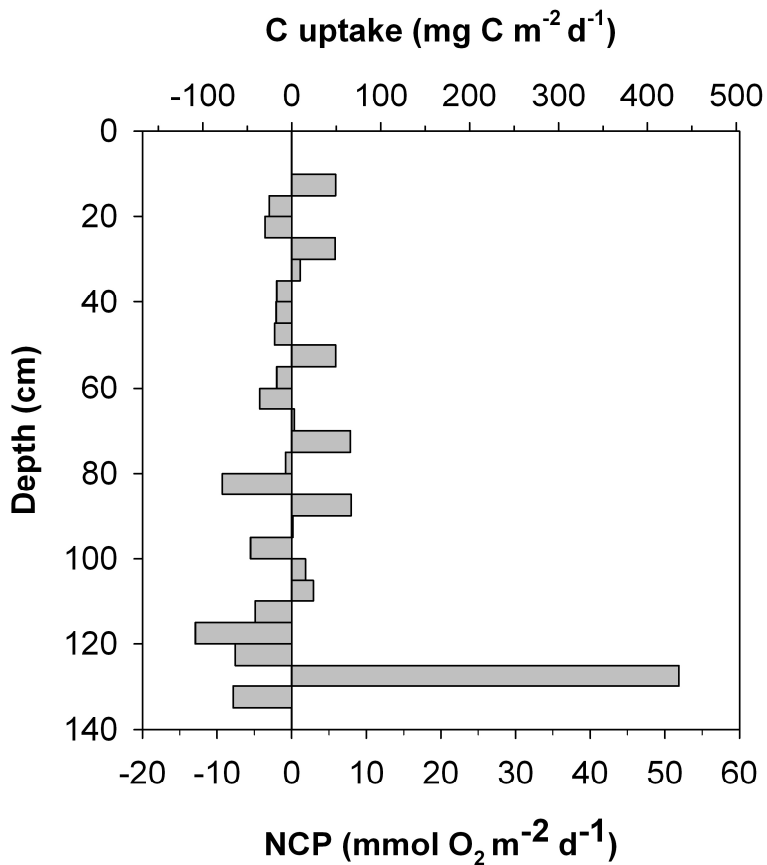


Fig. 6. NCP in BRW10 assuming equilibrium between the diffusion and NCP (see Sect. 4.3). The results were converted into C uptake, assuming a photosynthetic quotient O_2/C of 1.43 (Glud et al., 2002).